Pricing financial derivatives with exponential quantum speedup

Javier Gonzalez-Conde,[1,2,*] Ángel Rodríguez-Rozas,[3] Enrique Solano,[1,4,5,6] and Mikel Sanz[1,4,7,†]

[1]*Department of Physical Chemistry, University of the Basque Country UPV/EHU, Apartado 644, 48080 Bilbao, Spain*
[2]*Quantum Mads, Uribitarte Kalea 6, 48001 Bilbao, Spain*
[3]*Risk Division, Banco Santander, Avenida de Cantabria S/N, 28660 Boadilla del Monte, Madrid, Spain*
[4]*IKERBASQUE, Basque Foundation for Science, Plaza Euskadi 5, 48009, Bilbao, Spain*
[5]*International Center of Quantum Artificial Intelligence for Science and Technology (QuArtist) and Department of Physics, Shanghai University, 200444 Shanghai, China*
[6]*Kipu Quantum, Kurwenalstrasse 1, 80804 Munich, Germany*
[7]*IQM, Nymphenburgerstr. 86, 80636 Munich, Germany*

(Dated: June 28, 2021)

Pricing financial derivatives, in particular European-style options at different time-maturities and strikes, is a relevant financial problem. The dynamics describing the price of vanilla options when constant volatilities and interest rates are assumed, is governed by the Black-Scholes model, a linear parabolic partial differential equation with terminal value given by the pay-off of the option contract and no additional boundary conditions. Here, we present a digital quantum algorithm to solve Black-Scholes equation on a quantum computer for a wide range of relevant financial parameters by mapping it to the Schrödinger equation. The non-Hermitian nature of the resulting Hamiltonian is solved by embedding the dynamics into an enlarged Hilbert space, which makes use of only one additional ancillary qubit. Moreover, we employ a second ancillary qubit to transform initial condition into periodic boundary conditions, which substantially improves the stability and performance of the protocol. This algorithm shows a feasible approach for pricing financial derivatives on a digital quantum computer based on Hamiltonian simulation, technique which differs from those based on Monte Carlo simulations to solve the stochastic counterpart of the Black Scholes equation. Our algorithm remarkably provides an exponential speedup since the terms in the Hamiltonian can be truncated by a polynomial number of interactions while keeping the error bounded. We report expected accuracy levels comparable to classical numerical algorithms by using 10 qubits and 94 entangling gates to simulate its dynamics on a fault-tolerant quantum computer, and an expected success probability of the post-selection procedure due to the embedding protocol above 60%.

I. INTRODUCTION

In finance, European-style vanilla options are financial derivative contracts written on an underlying asset, which give the holder the right to buy or sell such asset on a specified future date at a predetermined strike price. One of the fundamental tasks of quantitative finance is calculating a *fair price* of such option contract before their expiration time. This task is far from being straightforward due to the randomness associated to the time evolution of both the underlying stock and the interest rates, whose dynamics can be modelled via either a stochastic processes or a partial differential equation, and connected by the celebrated Feynman-Kac formula. One of the first successful approaches to this problem was achieved by F. Black and M. Scholes in 1972, who proposed the celebrated Black-Scholes model [1], in which a lognormal distribution of the underlying stock price is assumed. Even though a closed-form solution exists for this dynamics, numerical solutions are still considered relevant since they serve as a benchmark for more sophisticated models. Numerical solutions also turn out to be fundamental when hedging a portfolio with a great number of coupled options. Several classical methods proposed in the literature includes finite differences, finite elements, Monte Carlo methods, and Fourier (spectral) methods [2–6].

Quantum technologies have experienced a rapid development in the last decade. Recently, Google has achieved quantum advantage, meaning that they have performed a calculation employing a superconducting processor faster than the most powerful supercomputers available today [7]. One of the fields which will expectably experience a deep impact due to this upcoming technology is finance. Indeed, the emergence of scalable quantum technologies will affect forecasting, pricing and data science, and will undoubtedly have an economic impact in the following years [8, 9]. Certainly, there already exist several efforts in this direction, for instance, an attempt to predict financial crashes [10, 11], the application of the principal component analysis to interest-rate correlation matrices [12], quantum methods for portfolio optimization [13–17], quantum generative models for finance [18], a quantum model for pricing collateral debt obligations [19], a protocol to optimize the exchange of securities and cash between parties [20], an application to improve Monte Carlo methods in risk analysis [21, 22], among many others. Regarding the option pricing problem, it has been studied the problem of solving Black-Scholes model employing Monte Carlo methods to solve the associated stochastic differential equation (SDE). In Ref. [23], the authors proposed a theoretical approach based on solving the SDE using quantum Monte Carlo with quadratic speedup. Afterwards, an experimental implementation in the IBM Tokyo quantum processor was attained in Refs. [24–26], employing a gate-based methodology to price options and portfolios of options. More recently, another approach to solve the SDE was proposed in [27], in which an unary representation of the asset value is used to

* Corresponding author: javier.gonzalezc@ehu.eus
† Corresponding author: mikel.sanz@ehu.eus

build a quantum algorithm for European-style option pricing. Another alternative perspective to deal with problems involving linear partial differential equations is by adapting quantum algorithms applied to existing numerical methods [28–30].

In this Article, we propose a quantum algorithm for solving the Black-Scholes partial differential equation on a quantum computer. We map Black-Scholes equation into a Schrödinger equation with a non-Hermitian Hamiltonian. In order to simulate its dynamics in a quantum processor [31–37], we embed it into an enlarged Hilbert space with one ancillary qubit. As a consequence of this embedding, which enables us to reproduce the dynamics of the non-Hermitian Black-Scholes Hamiltonian, we will need to post-select the result depending on the outcome of the ancillary qubit. Moreover, by introducing a second ancillary qubit, we transform the initial boundary condition into a periodic boundary condition. This allows us to improve the performance and stability of the algorithm by mitigating edge effects propagation, which leads to an improvement in the accuracy of the solution. In comparison with classical solution techniques, our algorithm remarkably provides an exponential speedup when computing the value of the contract for a fixed stock price since the number of terms in the Hamiltonian can be truncated with a polynomial number of terms while keeping the error bounded. After benchmarking our algorithm for a wide range of financial parameters, the simulations show a precision comparable to classical algorithms with a quantum circuit comprising 10 qubits and 94 entangling gates to simulate its dynamics in a fault-tolerant quantum computer, and furthermore, an expected success probability of the post-selection protocol above 60%.

II. BLACK-SCHOLES SCHRÖDINGER EQUATION

Under the assumption of constant interest rate and volatility, and provided certain ideal market conditions, Black-Scholes model is based on the possibility of building a perfect dynamic (short option) hedging portfolio strategy, known as *delta hedging*, which consists in holding, at each time, a number of shares equal to the derivative of the option price with respect to stock price. Therefore, the only risky (random) factor associated to portfolio dynamics is eliminated and the value of the portfolio agrees with the option value at any time. The pricing problem for a specific derivative contract, i.e. to determinate its present price $C(t=0,S)$, is given by the Black-Scholes PDE:

$$\frac{\partial C}{\partial t} + rS\frac{\partial C}{\partial S} + \frac{1}{2}\sigma^2 S^2 \frac{\partial^2 C}{\partial S^2} = rC, \tag{1}$$

together with the terminal condition for the price of the option given by the pay-off of the option contract , $C(T,S)$, defined at maturity time, T, for any plausible value of the underlying stock $S \geq 0$. Here, r represents the constant risk-free interest rate while σ is the constant volatility of the stock.

Black-Scholes equation has a similar structure to Schrödinger equation [38], which suggests the possibility of simulating such model in a quantum platform. To that end, we will rewrite the Black-Scholes equation in a Hamiltonian form. First, the change of variables $S = e^x$, $-\infty < x < \infty$, allows us to recover the unbounded position variable, leading to the equation

$$\frac{\partial C}{\partial t} + \left(r - \frac{\sigma^2}{2}\right)\frac{\partial C}{\partial x} + \frac{\sigma^2}{2}\frac{\partial^2 C}{\partial x^2} = rC. \tag{2}$$

Note that this equation is a backward parabolic equation. Let us now introduce the (momentum) operator $\hat{p} = -i\frac{\partial}{\partial x}$ to rewrite Eq. (1) as

$$\frac{\partial C}{\partial t} = -i\hat{H}_{BS}\, C \tag{3}$$

where

$$\hat{H}_{\mathrm{BS}} = i\frac{\sigma^2}{2}\hat{p}^2 - \left(\frac{\sigma^2}{2} - r\right)\hat{p} + ir\mathbb{I}. \tag{4}$$

Solutions to Eq. (3) are given by the propagator $\hat{U}(t) = e^{-it\hat{H}_{BS}}$ acting on the initial condition, $C(0,S)$, which, after a change of variables, propagates the solution forward in time from $t=0$ to T (i.e. effectively from the final condition defined at the physical time $t=T$ backwards to the the initial time $t=0$), $C(T,S) = \hat{U}(T)\, C(0,S)$. As observed from Eq. (4), this operator is a non-Hermitian operator, $\hat{H}_{BS} \neq \hat{H}_{BS}^{\dagger}$, which implies that neither its eigenvalues are necessarily real, nor the time evolution operator, $\hat{U}(t)$, is unitary.

The evolution of a closed quantum system is always unitary and hence, this fact supposes a major problem in terms of finding a physical system that evolves following the dynamics given by Black-Scholes model. To tackle this challenge our propagator is embedded into a larger space, employing afterwards a post-selection technique so that we effectively recover the desired Black-Scholes dynamics.

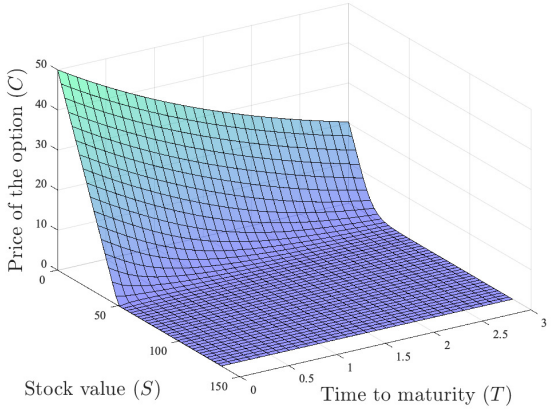

FIG. 1. Typical solutions of Eq. (1) for a Put-type option. Simulation parameters: $S_{\max} = 135$ u, $K = 50$ u, $\sigma = 0.2$, $r = 0.3$.

III. EMBEDDING PROTOCOL

Our non-Hermitian Hamiltonian can be decomposed into a Hermitian and an anti-Hermitian part, i.e., $\hat{H}_{\rm BS} = \hat{H}_{\rm BSH} + \hat{H}_{\rm BSA}$, with

$$\hat{H}_{\rm BSH} = -\left(\frac{\sigma^2}{2} - r\right)\hat{p}, \quad \hat{H}_{\rm BSA} = i\left(\frac{\sigma^2}{2}\hat{p}^2 + r\mathbb{I}\right). \tag{5}$$

Additionally, we have that $[\hat{H}_{\rm BSH}, \hat{H}_{\rm BSA}] = 0$, so the propagator $\hat{U}(t) = e^{-it\hat{H}_{\rm BSA}}\, e^{-it\hat{H}_{\rm BSH}}$. Furthermore, notice that $\hat{O}(t) = e^{-it\hat{H}_{\rm BSA}}$ is a Hermitian operator.

In order to circumvent the problem of dealing with the non-Hermitian operator. We embed the propagator $\hat{O}(t)$ into a larger unitary operator using a technique from operator theory called *unitary dilation* [39]. Indeed, by adding an ancillary qubit to our system, we can embed $\hat{O}(t)$ into the unitary operator $\tilde{U}(t)$ which can be written as

$$\tilde{U}(t) = \begin{pmatrix} \hat{O} & \sqrt{1-\hat{O}^2} \\ \sqrt{1-\hat{O}^2} & -\hat{O} \end{pmatrix} = \left(\hat{\sigma}^z_E \otimes \mathbb{I}\right) \exp\left(i\hat{\sigma}^y_E \otimes \tilde{H}(t)\right), \tag{6}$$

with $\tilde{H}(t) = \arccos(\hat{O}(t))$ and $\left\|\hat{O}\right\| \leq 1$.

Starting from an initial state $|\Phi_0\rangle = |0_E\rangle \otimes |\phi_0\rangle$, with $|\phi_0\rangle$ codifying the initial condition of the PDE (see section V A), the system evolves under the unitary operator $\tilde{U}(t)$ to obtain the state

$$|\Phi\rangle = \hat{O}\,|0_E\rangle \otimes |\phi_0\rangle + \sqrt{1-\hat{O}^2}\,|1_E\rangle \otimes |\phi_0\rangle\,. \tag{7}$$

A post-selection process which keeps only the outcomes with the ancillary qubit in the state $|0_E\rangle$ allows us to simulate the operator $\hat{O}(t)$ in a quantum computer, and in consequence, the whole Hamiltonian dynamics. We provide the details of the state preparation and post-selection process in section V.

IV. DIGITIZATION OF THE SPACE

In order to perform a digital simulation of the Black-Scholes equation using a quantum computer, it is required a discretization of position and momentum spaces based on the number of qubits employed. The possibility of simulating these financial models on a discretized space is guaranteed by the Nyquist-Shannon sampling theorem (see and Appendix VII A for details). Following the work in Ref. [40], a wave function $|\Psi\rangle$ such that $|\Psi(x)| < \epsilon$ when $|x| > L$ and whose Fourier transform $|\hat{\Psi}(p)| < \epsilon$ if $|p| > L$ can be sampled in position space using the basis of sampling vectors $\{|x_i\rangle_i\}$ where $x_i = -L + i\delta_x$, with $\delta_x \leq \frac{\pi}{L}$ and $i = 0, 1, ..., N_x - 1$ such that $x_i \in [-L, L]$. For a given interval, in the limit where $\delta_x = \frac{\pi}{L}$, the minimum N_x will be given by the equality $2L = \delta_x(N_x - 1)$. Hence, the wave function can then be rewritten as $|\Psi\rangle = \sum_{i=0}^{N_x-1} \Psi(x_i)\,|x_i\rangle$. The conjugate momentum basis is obtained by the discrete Fourier transform of the position basis $|p_k\rangle = \frac{1}{\sqrt{N}} \sum_{i=0}^{N_x-1} e^{ix_ip_k}\,|x_i\rangle$. These sampling basis allow us to define the following discretized position and momentum operators acting on their own basis, $\hat{X}_x\,|x_i\rangle = x_i\,|x_i\rangle$, $\hat{P}_k\,|p_k\rangle = p_k\,|p_k\rangle$.

For a space spanned by n_Q qubits, they will generate $N_x = 2^{n_Q}$ basis states, which means an exponential compression with respect to any classical algorithm which will lead to an exponential speed up if we can simulate the system employing a polynomial number of gates in terms of the number of qubits. Considering an equispaced grid of the interval $[-L, L]$, the position in such space can take the values $x = -x_{\max} + \delta_x\beta_x$, with $\delta_x = \frac{2x_{\max}}{N_x - 1}$ and $\beta_x = 0, \ldots, N_x - 1$. If we consider that the position $x = -x_{\max}$ is represented by the state $|0...0\rangle$, and the position $x = x_{\max}$ is represented by $|1...1\rangle$, the matrix form of this operator in the x basis is

$$\hat{X}_x = x_{\max}\begin{pmatrix} -1 & 0 & \ldots & 0 & 0 \\ 0 & -1+\delta_x & \ldots & 0 & 0 \\ \vdots & \vdots & \ddots & \vdots & \vdots \\ 0 & 0 & \ldots & 1-\delta_x & 0 \\ 0 & 0 & \ldots & 0 & 1 \end{pmatrix}. \tag{8}$$

Let us now construct the momentum operator. On the basis of finite differences, by using a Taylor expansion we define a second order approximation operator for the derivative as

$$\frac{d\mathrm{f}(x)}{dx} \approx \frac{\mathrm{f}(x+\delta_x) - \mathrm{f}(x-\delta_x)}{2\delta_x}. \tag{9}$$

Consequently, imposing periodic boundary conditions, the discrete momentum operator is given by the matrix

$$\hat{P}_x = \frac{-i}{2\delta_x}\begin{pmatrix} 0 & 1 & 0 & \ldots & 0 & -1 \\ -1 & 0 & 1 & \ldots & 0 & 0 \\ \vdots & \vdots & \vdots & \ddots & \vdots & \vdots \\ 0 & 0 & \ldots & -1 & 0 & 1 \\ 1 & 0 & \ldots & 0 & -1 & 0 \end{pmatrix}. \tag{10}$$

Therefore, conjugate squared momentum operator is given by the square of the previous matrix. Notice that canonical commutation relations between $\hat{x}$ and $\hat{p}$ are broken with the discretization. Momentum matrix $\hat{P}_x$ belongs to circulant matrix class, thus its diagonal form is achieved by using discrete Fourier transform matrix. In case that $|x\rangle$ is a space basis state, the quantum Fourier transform can also be expressed as the map QFT : $|x\rangle \mapsto \frac{1}{\sqrt{N}} \sum_{k=0}^{N-1} \omega_{N_x}^{xk}\,|p_k\rangle$, where $\omega_{N_x} = e^{\frac{2\pi i}{N_x}}$. So we can obtain the diagonal momentum operator by employing the Fourier transform,

$$\hat{P}_x = F^{\dagger}_{N_x}\hat{P}_k F_{N_x}. \tag{11}$$

The analytical expression of the eigenvalues of $\hat{P}_x$ is also known, and can be described by equation

$$p_k = \frac{\sin\left(\frac{2\pi k}{N_x}\right)}{\delta_x}, \quad k = 0 \ldots N_x - 1. \tag{12}$$

This simplifies considerably their implementation, provided that they are applied on the adequate space.

With this discretization of the sampling operators, $\hat{X}_x$ and $\hat{P}_k$, the solution to Black-Scholes equation obtained and its relative discretization error with respect to the analytical solution are depicted in Fig. 2 for different number of qubits.

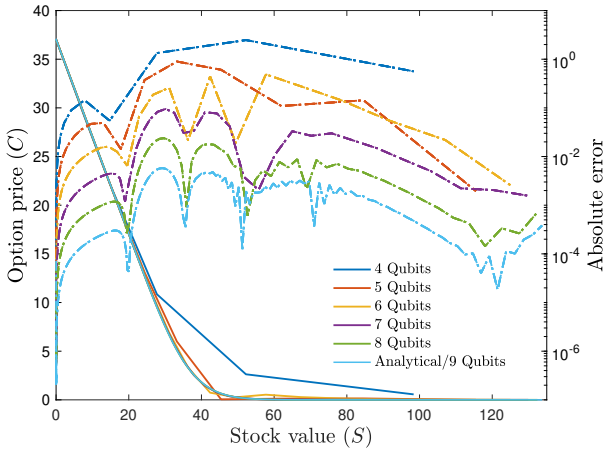

FIG. 2. Convergence of the solution of Black-Scholes put option pricing problem obtained with the finite differences discretezed operator $\hat{P}_x$ for distinct number of qubits, n_Q. Discretization error per point depending on the number of qubits, n_Q. Simulation parameters: $S_{\max} = 135$ u, $K = 50$ u, $\sigma = 0.2$, $r = 0.3$, $T = 1$ year.

V. QUANTUM CIRCUIT IMPLEMENTATION

In this section, we show the different components of the circuit which simulates the price evolution of a put option in a quantum computer (the procedure for a call option would be similar but initializing the process in the right state). We depict a general overview of the quantum circuit in Fig. 3, and in the following sections, we explain in detail every block acting on the $n_Q + 2$ qubits.

A. Boundary Conditions and Initial state

The pricing problem of an European put option is given by Black-Scholes equation plus a boundary condition depending on the strike price, K, at the maturity time, T,

$$C(T, S) = \max\{K - S, 0\}. \tag{13}$$

In order to solve the boundary value problem, we revert time, $t \to T - t$, so the boundary condition transforms into an initial one, and hence we deal with an initial value problem.

Additionally, due to the choice of boundary conditions for momentum operator in Eq. (10), we make use of one of the

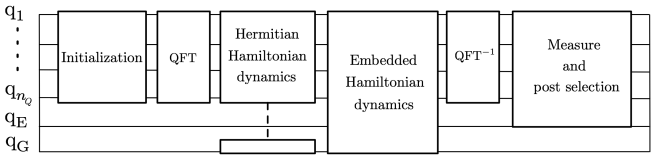

FIG. 3. General overview of the circuit that accomplish Black-Scholes digital simulation. In the first step of the circuit, we obtain the initial state which encodes the payoff condition of the corresponding option type. Then, we apply the quantum Fourier transform (QFT) that enables us to work in the momentum space. We implement both sets of gates from Hermitian and non-Hermitian dynamics using an ancilla qubit q_G. In the case of non-Hermitian dynamics, an embedding qubit, q_E, is also required. In order to recover the information in position space, we operate with inverse quantum Fourier transform and, in the end, we perform the measure and post-selection protocol.

n_Q qubits to duplicate the initial condition in the x space in order to impose periodic boundary conditions which mitigate border effects. The solution is hence given in the interval $(-x_{\max}/2, x_{\max}/2)$. In the case of the put option, we encode this condition into the initial quantum state as

$$|\phi_0\rangle = \sum_{j=0}^{N_{\max}} \frac{K - e^{-x_{\max}/2 + j\delta_x}}{\Lambda^{1/2}} \left(|x_j\rangle + |x_{N_x - 1 - j}\rangle \right), \tag{14}$$

with

$$N_{\max} = \left\lfloor (N_x - 1) \left(\frac{\log(K)}{2x_{\max}} + \frac{1}{4} \right) \right\rfloor, \quad \Lambda = \left(2 \sum_{m=0}^{N_{\max}} (K - e^{-x_{\max}/2 + m\delta_x})^2 \right). \tag{15}$$

Moreover, we need two additional ancillary qubits associated with the embedding and the optimal implementation of quantum gates. The initial state of the embedded system is therefore $|\Phi_0\rangle = |0_G\rangle \otimes |0_E\rangle \otimes |\phi_0\rangle$.

In the general case, loading an arbitrary state into a quantum computer requires an exponential quantity of gates [41–47], which is inefficient and destroys any possible quantum advantage. Nevertheless, for some specific cases such as smooth differentiable functions, integrable or log-concave probability distributions, as is our case (see Appendix VII C), they can be efficiently loaded into a gate-based quantum computer, as detailed in [48, 49]. The authors proved a requirement of an exponentially small entanglement entropy for each added qubit to represent this kind of functions, and consequently in the number of two qubit gates demanded. In order to obtain an explicit circuit that implements the initialization quantum Generative Adversarial Networks (qGAN) have been proposed to load a distribution using a polynomial number of gates via a variatonal ansatz [50].

B. Quantum Fourier Transform

As Black-Scholes Hamiltonian only depends on the momentum operator $\hat{P}_x$, we employ the quantum Fourier trans-

form in the circuit to change the basis from position one, which codifies the initial state, to the momentum basis, which considerably simplifies the circuit. Indeed, we want to simulate operators $\hat{O}(t)$ and $e^{-it\hat{H}_{\rm BSH}}$. By using Eq.(11) and the identity, $f\left(F_{N_x}^{\dagger}\hat{P}_k F_{N_x}\right) = F_{N_x}^{\dagger} f\left(\hat{P}_k\right) F_{N_x}$, where f is an analytic function, the problem reduces itself to calculate the exponential of operator functions acting on diagonal momentum matrices. To sum up, an initial Fourier transform allows us to transform the initial condition in positions basis, Eq. (13), into the momentum space. After applying the diagonal operators, the inverse Fourier transform will enable us to recover the solution in position space. Therefore, we can assume from now on that the operators are diagonal.

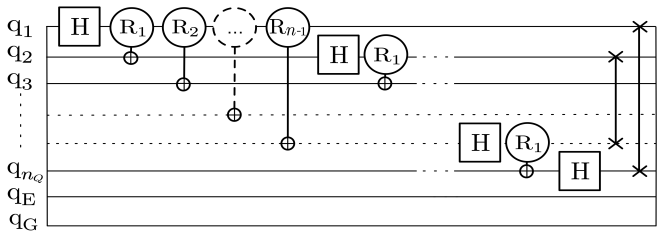

FIG. 4. The circuit of the quantum Fourier transform for n_Q qubits. Due to the introduction of periodic boundary conditions, this circuit substantially reduces the border effects. Once we have performed all the controlled rotations, it is necessary to swap all the qubits in order to retrieve the initial indexing in the momentum space. The used logic gate R_m corresponds to the control phase gate $\mathrm{R}(\phi = \frac{\pi}{2^m})) = \mathrm{diag}(1, 1, 1, \exp(i\phi))$.

C. Gates of Hamiltonian dynamics

Once we have the expression for the eigenvalues of $\hat{P}_k$, Eq. (12), we rewrite both Hamiltonians $\hat{H}_{\rm BSH}$ and $\tilde{H}$ in the Cartan basis. This helps us to find the logic gates to implement the corresponding qubit operators. Let us first focus on the non-Hermitian part, $\tilde{H}$. The Hamiltonian of the embedded time evolution operator is given by

$$\tilde{H} = f\left(-T\left(\frac{\sigma^2}{2}\hat{P}_k^2 + r\mathbb{I}\right)\right), \tag{16}$$

where $f(x) = \arccos(\exp(x))$. Hence, we can use the spectral theorem to decompose the Hamiltonian into projectors basis

$$\tilde{H} = \sum_{k=0}^{N_x-1} \underbrace{f(-T(\frac{\sigma^2}{2}p_k^2 + r))}_{h_k} |p_k\rangle\langle p_k|, \tag{17}$$

where p_k is given by Eq. (12). For the case of the Hermitian Hamiltonian, the decomposition corresponds to

$$\hat{H}_{\rm BSH} = \sum_{k=0}^{N_x-1} \underbrace{-\left(\frac{\sigma^2}{2} - r\right)p_k}_{h_k} |p_k\rangle\langle p_k|. \tag{18}$$

By rewriting $\hat{P}_k$ in terms of the Cartan basis, we obtain

$$\tilde{H} = \sum_{i_0\ldots i_{n_Q-1}=0}^{1} \underbrace{\left(\frac{1}{N_x}\sum_{k=0}^{N_x-1} h_k W_I\left(\frac{k}{N_x}\right)\right)}_{h'_I} \underbrace{\hat{\sigma}_0^{i_0}\ldots\hat{\sigma}_{n_Q-1}^{i_{n_Q-1}}}_{\hat{c}_I}, \tag{19}$$

where $\hat{\sigma}_j^0 = \mathbb{I}_j$, $\hat{\sigma}_j^1 = \hat{\sigma}_j^z$ denotes the operator acting on qubit j, $j = 0, ..., n_Q - 1$, and $W_I(x)$ is the I-th Walsh function with $I = \sum_{j=0}^{n_Q-1} i_j 2^j$ (see Appendix VII D). A similar expression is obtained in the Hermitian case.

The product $\hat{\sigma}_E^y \otimes \tilde{H}$ is given by a sum of commuting observables, so its exponential can be divided into a product of exponentials. An analogue process leads us to achieve the Hermitian decomposition in Cartan basis.

Now, we provide the gates [51] to simulate an unitary operator of the form

$$U = e^{i\beta\ \hat{\sigma}_E^y \otimes (\hat{\sigma}_{i_1}^z \ldots .\ \hat{\sigma}_{i_k}^z)} \tag{20}$$

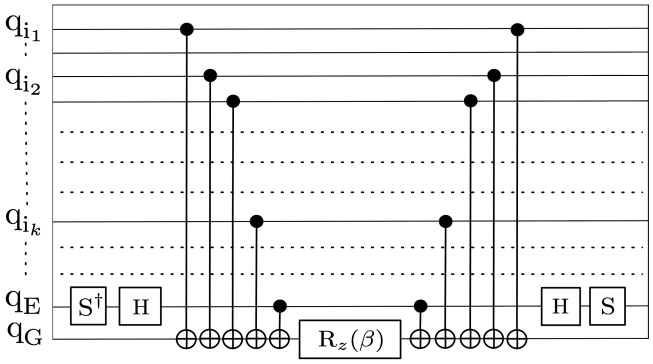

FIG. 5. Circuit implementation of operator in Eq. (20). The main idea behind this construction is to encode the parity of the involved qubits into the ancilla-gate qubit, $\mathrm{q_G}$, so this qubit accomplish a rotation depending on that. The construction of the whole circuit involves as many of these terms as vectors of the Cartan basis are included in the description of our Hamiltonian.

D. Depth of the circuit

In the general case, the decomposition of each Hamiltonian in the Cartan basis leads to $N_x = 2^{n_Q}$ qubit interactions. Translated into logic gates in an optimized circuit, it means around 2^{n_Q+1} entangling gates. Due to the symmetry (embedded Hamiltonian) and antisymmetry (Hermitian Hamiltonian) of the eigenvalues h_k, we can reduce this quantity to 2^{n_Q}. Unfortunately, this is still excessive and destroys the speedup achieved by the position codification.

The question that we address in this section is whether it is possible to truncate the number of terms without substantially affecting the accuracy of the algorithm. Let us firstly focus on the Hermitian term since, as we will see at the end of this section, its truncation error will dominate the total error. In this case, due to the antisymmetry of the eigenvalues, every non-zero term must include $\hat{\sigma}^z_0$. Additionally, interactions with an odd number of bodies are in general the largest ones. For each non-zero term, Eq. (19) sums up to an analytical expression. We split the expressions into three categories: only first qubit interaction, interactions with an odd number of bodies, and interactions with an even number of bodies. Denoting by $0 = j_0 < j_1 < j_{2k} \leq n_Q - 1$ the indices of the qubits on which the operators act, the reindexed coefficients h'_J of Eq. (19) are

$\underline{\hat{\sigma}^z_0\, \mathbb{I}_1 \dots \mathbb{I}_{n_Q-1}}$:

$$\frac{2^{n_Q}-1}{2^{n_Q+1}} \frac{2r-\sigma^2}{x_{\max}} \cot\left(\frac{\pi}{2^{n_Q}}\right). \tag{21}$$

$\underline{\hat{\sigma}^z_{j_0=0}\hat{\sigma}^z_{j_1} \dots \hat{\sigma}^z_{j_{2k}}}$:

$$(-1)^k \frac{2^{n_Q}-1}{2^{n_Q+1}} \frac{2r-\sigma^2}{x_{\max}} \cot\left(\frac{\pi}{2^{n_Q}}\right) \tan\left(\frac{\pi}{2^{j_1+1}}\right) \dots \tan\left(\frac{\pi}{2^{j_{2k}+1}}\right). \tag{22}$$

$\underline{\hat{\sigma}^z_{j_0=0}\hat{\sigma}^z_{j_1} \dots \hat{\sigma}^z_{j_{2k-1}}}$:

$$(-1)^k \frac{2^{n_Q}-1}{2^{n_Q+1}} \frac{2r-\sigma^2}{x_{\max}} \tan\left(\frac{\pi}{2^{j_1+1}}\right) \dots \tan\left(\frac{\pi}{2^{j_{2k-1}+1}}\right). \tag{23}$$

We can check from Eqs. (22) and (23) that the arguments of the tangent functions verify $0 \leq \frac{\pi}{2^{j_l+1}} \leq \pi/4$ for $l = 1 \dots 2k$. Hence, we have the inequality $\tan\left(\frac{\pi}{2^{j_l+1}}\right) \leq \frac{4}{2^{j_l+1}}$ due to the convexity of the tangent function. For a fixed n, considering the previous inequality, we obtain the upper bound

$$\tan\left(\frac{\pi}{2^{j_1+1}}\right) \dots \tan\left(\frac{\pi}{2^{j_{2k}+1}}\right) \leq \frac{1}{2^{\sum_{l=1}^{2k}(j_l-1)}}, \tag{24}$$

Following the previous expression, let us now define the index $I' = \sum_{l=1}^{2k}(j_l - 1)$ for the terms which have an odd number of body interactions. Notice from Eqs. (22) and (23), that for every term with an even number of body interactions not ending in $\hat{\sigma}^z_{n_Q-1}$, there exists a term with an odd number of body interactions ending in $\hat{\sigma}^z_{n_Q-1}$ with the same value, hence it inherits the index I'. To complete the reassignment, we need to define the value of index I' for those terms with an even number of body interactions ending in $\hat{\sigma}^z_{n_Q-1}$. For such purpose, we increase the number of qubits one unit, and consider the term as part of this system with a larger quantity of qubits not including the interaction with the last one, so we already know how to calculate its index in this new scenario. To recover the index in the original system, consider then that the index of a term with an even number of body interactions increases one unit when the size of the system is increased in one qubit, it is $I'_{n_Q+1}(\hat{\sigma}^z_{j_0=0}\hat{\sigma}^z_{j_1} \dots \hat{\sigma}^z_{j_{2k-1}}) = I'_{n_Q}(\hat{\sigma}^z_{j_0=0}\hat{\sigma}^z_{j_1} \dots \hat{\sigma}^z_{j_{2k-1}}) + 1$. We conclude from Eq. (24) that with this realignment if the index of a certain term is $I'(J) = I'$, hence $|h'_J|$ is upper bounded by $|h'_J| \leq Ce^{-\log(2)I'}$, where C is a constant depending on n_Q and the financial parameters ($C = \frac{2^{n_Q}-1}{2^{n_Q+1}} \frac{2r-\sigma^2}{x_{\max}} \cot\left(\frac{\pi}{2^{n_Q}}\right)$). Notice that this reassignment is non-bijective, hence we denote $g_{I'}$ as the degeneration of the index [52] (see Appendix VII F). We define M as the Mth largest value of index I'.

We have now all necessary elements to prove that the error after truncating the first M index terms is exponentially supressed with M. Indeed, in order to quantify the error corresponding to the truncation from M-th term, we analyze the norm $\left\| e^{iT\sum_{I'=M}^{\frac{n_Q}{2}(n_Q-1)-1} \sum_{J|I'(J)=I'} h'_J \hat{c}_J} - e^{i\theta}\mathbb{I} \right\|_\infty$ (see Appendix VII F). In the worst case escenario, the maximum rotation angle between two eigenstates would be $\sum_{I'=M}^{\frac{n_Q}{2}(n_Q-1)-1} \sum_{J|I'(J)=I'} |h'_J| \leq C \sum_{I'=M}^{\frac{n_Q}{2}(n_Q-1)-1} \frac{g_{I'}}{2^{I'}} < \frac{2C'}{2^M}$, with C' a new constant depending on n_Q and the financial parameters (see Appendix VII F). This rotation is evenly distributed, hence the optimal gauge election is $\theta = 0$.

Consequently, taking M sufficiently large to guarantee that $C'e^{-\log(2)M} \leq \pi/4$, we get the following upper bound for the error

$$\left\| e^{iT\sum_{I'=M}^{\frac{n_Q}{2}(n_Q-1)-1} \sum_{J|I'(J)=I'} h'_J \hat{c}_J} - e^{i\theta}\mathbb{I} \right\|_\infty \leq \sqrt{2\left(1-\cos(2TC'e^{-\log(2)M})\right)}, \tag{25}$$

where $\hat{c}_J$ is the vector of the Cartan basis corresponding to the coefficient h'_J (notice that $\|\hat{c}_J\|_\infty = 1\ \forall j$). We conclude that, for an error ϵ, we can truncate our Hamiltonian in a polynomial number of terms, $M \leq \log_2(2TC') + \log_2(\arccos(1 - \epsilon^2/2))$ (see Appendix VII G), without substantially affecting the accuracy of the algorithm.

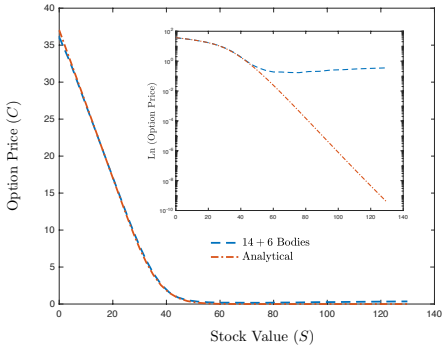

FIG. 6. Solution to Black-Scholes equation obtained by considering the largest 14 terms of the Hermitian Hamiltonian and the largest 6 interactions of the embedded. We compare it with the analytical solution evaluated in the same grid points. The inset shows both curves in a logarithmic scale, what enables us to appreciate the difference. Simulation parameters: $S_{\max} = 135$ u, $K = 50$ u, $\sigma = 0.2$, $r = 0.3$, $T = 1$ year, $n_Q = 8$.

Finally, we will show that the truncation error of the Hermitian Hamiltonian effectively dominates the error. In the em-

bedded case, we were not able to find close analytic results for the sums defining the coefficients, but asymptotic expressions for large n_Q, which are shown in Appendix VII E. Indeed, these expressions show that, for sufficiently large n_Q, the Mth term of the embedded Hamiltonian is much smaller than the Mth term of the Hermitian Hamiltonian. Consequently, the truncation error of the former is upper bounded by the one of the other. As an illustration of these results, we have studied the case $n_Q = 8$, since it already provides a discretization comparable to the standard classical case. For the case of $n_Q = 8$, this analysis leads us to find an optimal truncation to implement the algorithm. We propose to use the largest 14 terms of the Hermitian Hamiltonian and the 6 largest of the embedded one. In terms of gates, it means 94 entangling gates to simulate its dynamics, which is feasible in current quantum processors [7]. The solution obtained is compared with the analytical solution in Fig. 6. Also for $n_Q = 8$, we show in Fig. 7 that terms of the Hermitian Hamiltonian are considerably larger for the most relevant financial values. Furthermore, we study all the possible combinations of truncations in Fig. 8, showing that error strongly depends on the number of terms from the Hamiltonian, hence this Hamiltonian indeed dominates the dynamics.

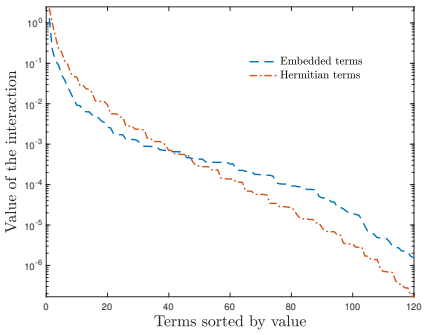

FIG. 7. Hermitian and embedded interactions terms sorted by absolute value represented in a logarithmic scale. For the most significant values, Hermitian terms dominate over embedded ones. Simulation parameters: $n_Q = 8$, $S_{\max} = 135$ u, $K = 50$ u, $\sigma = 0.2$, $r = 0.3$, $T = 1$ year.

E. Measurement and Post selection

Finally, the outcomes of the measurements in our circuit must be postselected in order to recover the non-Hermitian dynamics of Black-Scholes equation. Indeed, we firstly measure the ancillary embedding qubit, if it is $|0_E\rangle$, then we retrieve the price information, otherwise, we discard it. In order to retrieve the price information corresponding to the spot of interest $|x_i\rangle$, we proceed to measure the POVM$\left\{ |x_i\rangle\langle x_i|, \mathbb{I} - |x_i\rangle\langle x_i| \right\}$. This task can efficiently be attained by using a multi-control gate acting on an extra qubit. The probability of recovering the desired dynamics depends on the expression

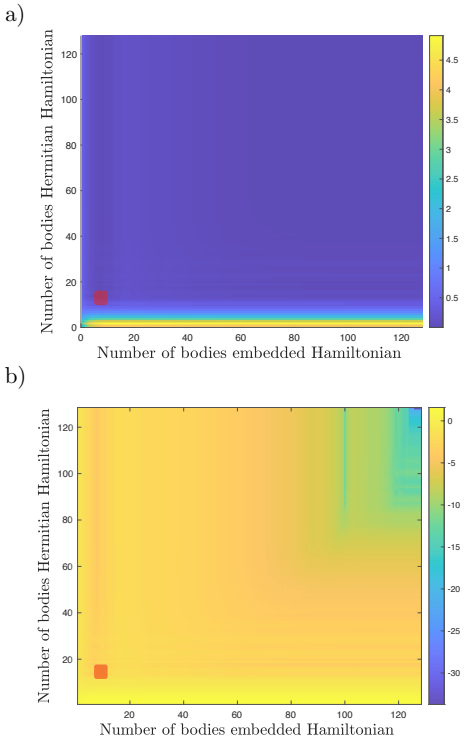

FIG. 8. Truncation error: a) Relative error of the approximated solution choosing the largest M terms with respect to the analytical solution calculated via L^1-norm. b) Logarithmic relative error of the approximated solution choosing the largest M terms respect to the analytical solution calculated via L^1-norm. Simulation parameters: $S_{\max} = 135$ u, $K = 50$ u, $\sigma = 0.2$, $r = 0.3$, $T = 1$ year, $n_Q = 8$.

$$Ps = \langle\phi_0| QFT' e^{-2T(\frac{\sigma^2}{2}\hat{P}_k^2 + r\mathbb{I})} QFT |\phi_0\rangle . \tag{26}$$

This success probability strongly depends on the maturity time and risk-free interest rate but, for the usual range of financial parameters its value is always above 0.6, as depicted in Fig. 9. Therefore, we only need to double the number of runs of the algorithm, which does not change its polynomial behaviour. Assuming the constraint $e^{x_{\max}/2} = 3K$, it is possible to obtain a lower bound $Ps \geq e^{-2Tr}\gamma(N_x, K)$. The function $\gamma(N_x, K)$, depicted in Fig. 10, shows an asymptotic behaviour when $N_x \to \infty$,

$$\lim_{N_x\to\infty} \gamma(N_x, K) = \frac{\left(-1 + K^2 - 6K^2\log(K)\right)^2}{(-1 + 12K^2 - 11K^4 + 36K^4\log(K))\log(3K)}. \tag{27}$$

At time $T = 0$, $\gamma(N_x, K)$ converges when $N_x \to \infty$ to a relative lower bound of the area under the initial condition.

Finally, the discrete solution for the Black-Scholes equation at maturity time, T, is given by the expression

$$C(T, x_i) = \sqrt{p(x_i|0_E)\Lambda}, \tag{28}$$

where $p(x_i|0_E)$ is the probability of measuring the eigenstate

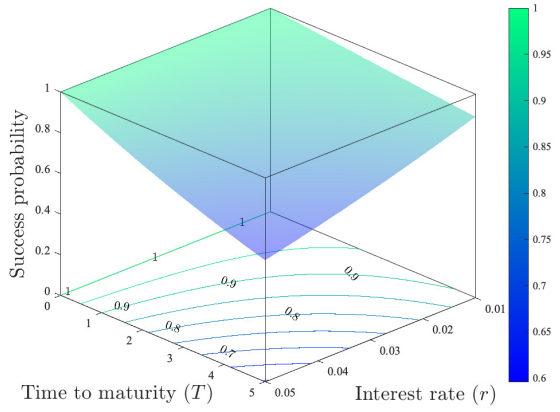

FIG. 9. Success probability in post-selection protocol corresponding to Eq. (26) depending on time to maturity in years and risk-free interest rate. The probability is above 0.6 for all values in the mesh. Parameters values: $S_{\max} = 150$ u, $K = 50$ u, $\sigma = 0.2$, $n_Q = 8$.

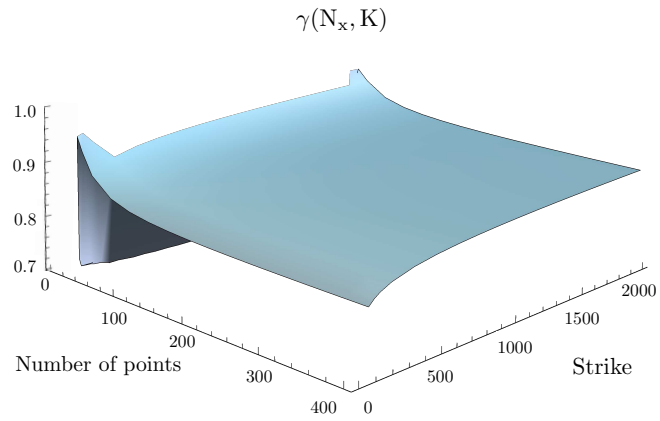

FIG. 10. Lower bound probability of success $\gamma(N_x, K)$. As we can observe there exists an asymptotic convergence value for both, number of points and strike, this value is always over 0.6 what indicates that our protocol would be success in more than a half of the realizations.

$|x_i\rangle$ conditioned to have obtained the state $|0_E\rangle$ in the embedding qubit and Λ is given by Eq. (15).

F. Time and stock-price-dependent volatility

We have considered a constant volatility, but our algorithm is straightforwardly adaptable to introduce a time dependance in volatility. This fact allows us to reproduce more complex financial models such as Heath–Jarrow–Morton. In the general case time dependent volatility expression is given by an interpolation among equispaced known values. The introduction of this assumption means a slight change in the algorithm, the only difference in the coefficients decomposition is experimented in Eqs. (17) and (18) where the coefficient h_k turns into

$$-\left(\frac{\frac{1}{T}\int_0^T \sigma^2(t)}{2} - r\right) p_k \quad \text{and} \quad f\left(\frac{\int_0^T \sigma^2(t)}{2} p_k^2 + rT\right) \tag{29}$$

for the Hermitian and embedded Hamiltonian, respectively. Thus, the mean value theorem for definite integrals guarantees that the average value $\bar{\sigma^2} = \frac{1}{T}\int_0^T \sigma^2(t)$ is lower and upper bounded. This enables us to focus our study only in a bounded interval for the volatility, as we have done by now.

Regarding the case of a stock price-dependent-volatility, we can introduce a perturbation $\sigma_1(\hat{x})$ of order ϵ around a constant value σ_0. The diagonalization of $\sigma_0\mathbb{I} + \epsilon\hat{\sigma}_1(\hat{x})$ can be obtained via quantum Fourier transform with a deviation of order ϵ in the eigenvalues, what enables us to continue applying our protocol while keeping the error bounded and an exponential speed up. We remark that, for this case there exists no analytical solution to the PDE, therefore our algorithm would provide a meaningful numerical solution. This case will be studied in detail in further works.

VI. CONCLUSIONS

We have introduced a quantum algorithm to numerically solve Black-Scholes partial differential equation in a digital quantum computer by mapping it to Schrödinger equation. The non-Hermitian nature of the resulting Hamiltonian has been solved by embedding the dynamics into an enlarged Hilbert space, and by post-selecting the outcome of the simulation. In order to improve the stability and performance of our algorithm, we added an additional ancillary qubit to transform the initial condition into a periodic boundary condition. We have described its implementation for a wide range of relevant financial parameters in terms of qubit operators and quantum gates. Even though the number of terms resulting from the decomposition of the Hamiltonian in the computational basis grows exponentially with the number of qubits, we have been able to identify that only a polynomial number of interactions plays a relevant role to achieve an accurate solution, providing a remarkable exponential speedup when the price of the option is evaluated for a fixed stock price. Indeed, we have obtained a precision comparable to classical algorithms with a total of 10 qubits and 94 entangling gates to simulate its dynamics in a fault-tolerant quantum computer and an expected success probability value for the post-selection protocol above 60%. Our perspective for a future work is to introduce gate errors associated to NISQ devices in order to analyze the realistic implementation in a near-term quantum platform. We want to highlight that the embedding techniques introduced may be extended to simulate the dynamics of the general non-Hermitian Hamiltonians and imaginary time evolution. This could allow us to introduce additional degrees of freedom in the model, e.g. spatial-time dependent volatility (stochastic local volatility) or coupled options. For instance, we could use the quantum principal component analysis raised in Ref. [12] together with coupled Black-Scholes models to address

problems with coupled options. Moreover, the present work has been accomplish for the European option pricing problem, but it may be carried through simulate different kind of options, considering American and Asiatic options, for example.

ACKNOWLEDGEMENTS

We thank Bruno Candelas for useful discussions regarding the digital implementation. Authors acknowledge financial support from Spanish Government PGC2018-095113-B-I00 (MCIU/AEI/FEDER, UE), Basque Government IT986-16, as well as from QMiCS (820505) and OpenSuperQ (820363) of the EU Flagship on Quantum Technologies, EU FET Open Grant Quromorphic (828826), EPIQUS (899368) and Shanghai STCSM (Grant No. 2019SHZDZX01-ZX04) . This work is supported by the U.S. Department of Energy, Office of Science, Office of Advanced Scientific Computing Research (ASCR) quantum algorithm teams program, under field work proposal number ERKJ333.

VII. APPENDIX

A. Nyquist-Shannon sampling Theorem

Nyquist-Shannon sampling Theorem is a central part of our method, as well as it has a remarkably importance in signal processing, communications, and data compression.

Theorem VII.1 (**Nyquist-Shannon sampling).** *Let be* $F(x) : \mathbb{R} \to \mathbb{R}$ *a real function that has support in* $x \in [0, x_{max}]$ *in position space and between* $k = -k_{max}$ *and* $k = +k_{max}$ *in momentum space. Consider a discrete sampling of* $F(x)$ *over the interval* $x \in [0, L]$ *with* $L > x_{max}$ *and at intervals of* $\delta_x < \frac{\pi}{k_{max}}$. *Then the theorem ensures that* $F(x)$ *can be reconstructed up to corrections that are exponentially small.*

Under some assumptions, the theorem allows us to reconstruct a function via discretization introducing only exponentially small errors, as long as the function is sampled in both momentum and position space over the whole region where it has support. Nevertheless, there is a constraint arising from the theorem. The lattice spacing x must be small enough in order to discretize states with high momentum. It is also derived that the functions we will try to simulate should be restricted to some area in both momentum and position space.

B. Boundary conditions

When solving the Black-Scholes equation Eq. (1) after the change of variables $x = \log S$, the resulting equation, Eq. (2), turns out to be homogeneous with respect to x. In particular, this means that we can displace the initial condition by a given shift and solve the problem, in the sense that the actual solution of the original problem can be recovered afterwards by performing the same shift in the opposite direction. Indeed, given a bounded interval for the stock price $S \in [1/S_{max}, S_{max}]$, we make use of this property in order to have a symmetric initial condition with respect to x as follows: we make a shift in order to translate the initial condition of the Put such that the support of this initial condition is the interval $[0, 2\log S_{max},]$, instead of $[-\log S_{max}, \log S_{max}]$, for the given discretization. After this shift, we make a reflection in order to obtain periodic boundary conditions, we detail this procedure in the next section.

C. Initial State

Black-Scholes time reverted initial value problem starts from the initial condition. In terms of x, this condition results

$$C(T, x) = max\{K - \exp(x), 0\}. \tag{30}$$

Assuming that we use n_Q qubits to discretize x, hence we have $N_x = 2^{n_Q}$ points (eigenstates), each one of them corresponding to a discrete value of x_i.

$$x_i = -x_{\max} + \delta_x i \quad i = 0 \dots N_x - 1, \tag{31}$$

$$\hat{X}\,|x_i\rangle = x_i\,|x_i\rangle \quad i = 0 \dots N_x - 1, \tag{32}$$

where $\delta_x = \frac{2x_{\max}}{N_x - 1}$. Now we have to find which is the largest index i such that $K - \exp(x_i) \geq 0$, we call this value $N_{\max}$

$$K - \exp(x_{N_{\max}}) = 0 \to -x_{\max} + \delta_x N_{\max} = \log(K), \tag{33}$$

hence

$$N_{\max} = \left\lfloor (N_x - 1)\left(\frac{\log(K)}{2x_{\max}} + \frac{1}{4}\right)\right\rfloor \tag{34}$$

To encode this information into the quantum state, we associate the normalized and discretized value of the initial condition $C(T, x_i)$ to the probability amplitude of the corresponding eigenstate $|x_i\rangle$. Therefore, except normalization of the wave function, the coefficient (probability amplitude) of the eigenstate $|x_i\rangle$ is

$$K - \exp\left(-x_{\max} + \delta_x i\right)$$

for $i = 0....N_{\max}$

If we now use one of the n_Q qubits to duplicate the initial condition, then we have to consider some aspects. First of all, we impose symmetry of the wave function respect to x=0, hence

$$\text{coefficient}(|x_i\rangle) = \text{coefficient}(\left|x_{N_x - 1 - i}\right\rangle) \quad \forall i = 0....N_x - 1. \tag{35}$$

Furthermore, this duplication reduces the size of the real price simulation space to the interval $(-x_{\max}/2, x_{\max}/2)$, which is shifted to the interval $(-x_{\max}, 0)$ as we pursue to duplicate the initial condition respect to x=0, thus we recalculate the value $N_{\max}$

$$K - \exp(x_{N_{\max}}) = 0 \rightarrow -\frac{x_{\max}}{2} + \delta_x N_{\max} = \log(K), \tag{36}$$

thus

$$N_{\max} = \left[(N_x - 1)\left(\frac{\log(K)}{2x_{\max}} + \frac{1}{4} \right) \right]. \tag{37}$$

Therefore, except normalization of the wave function, the coefficient of the eigenstate $|x_i\rangle$ is

$$K - \exp(-x_{\max}/2 + \delta_x i),$$

for $i = 0....N_{\max}$. Considering that due to the duplication each coefficient is repeated twice, the norm squared results to be

$$\Lambda = \left(2 \sum_{m=0}^{N_{\max}} (K - \exp(-x_{\max}/2 + \delta_x m))^2 \right).$$

Finally the normalized wave function is

$$|\phi_0\rangle = \sum_{i=0}^{N_{\max}} \frac{K - e^{-x_{\max}/2 + \delta_x i}}{\Lambda^{1/2}} \left(|x_i\rangle + \left| x_{N_x - 1 - i} \right\rangle \right) = \sum_{i=0}^{N_x - 1} c_i(K) |x_i\rangle . \tag{38}$$

We can observe that this wave normalized function corresponds to the discretization of the normalized function f

$$\mathrm{f}(x) = \begin{cases} K - e^{x + x_{\max}/2} & \text{if } x \in (-2x_{\max}, \ln(K) - x_{\max}/2) \\ K - e^{-x + x_{\max}/2} & \text{if } x \in (x_{\max}/2 - \ln(K), 2x_{\max}) \end{cases}$$

which can be straightforwardly checked to be a log-concave function,

$$\ln(\mathrm{f}(x))'' = -\frac{e^{x_{\max}/2 + x} K}{(e^{x - \max/2} - e^x K)^2} < 0$$

$$\forall x \in (-2x_{\max}, \ln(K) - x_{\max}/2) \cup (x_{\max}/2 - \ln(K), 2x_{\max}).$$

D. Hamiltonian Change of Basis and Walsh Functions

In this section we present how to express our Hamiltonian in terms of Cartan basis. Suppose that we have a Hamiltonian expressed in terms of the canonical (projector) basis

$$H = \sum_{k=0}^{N_x - 1} h_k |k\rangle \langle k| . \tag{39}$$

We calculate the coefficient of the projector $|k\rangle\langle k|$ in the $\sigma_0^{i_0} ... \sigma_{n_Q-1}^{i_{n_Q-1}}$ element of the Cartan basis as

$$\frac{1}{N_x} \mathrm{tr}\left(|k\rangle\langle k| \, \sigma_0^{i_0} ... \sigma_{n_Q-1}^{i_{n_Q-1}} \right) = \frac{1}{N_x} \langle k| \, \sigma_0^{i_0} ... \sigma_{n_Q-1}^{i_{n_Q-1}} \, |k\rangle$$

$$= \frac{1}{N_x} \left\langle x_0 ... x_{n_Q-1} \right| \sigma_0^{i_0} ... \sigma_{n_Q-1}^{i_{n_Q-1}} \left| x_0 ... x_{n_Q-1} \right\rangle = \frac{1}{N_x} (-1)^{\sum_{j=0}^{n_Q-1} x_j i_j}, \tag{40}$$

where $k = \sum_{j=0}^{n_Q-1} x_j 2^{n_Q-1-j}$ and we define $x = \frac{k}{N_x} = \sum_{j=0}^{n_Q-1} x_j 2^{-1-j}$ as the fraction with the same binary representation. Now we present Walsh Functions in order to understand the change of basis from canonical projectors basis to Cartan basis. We define the family of Walsh Functions as:

$$W_I : [0, 1] \rightarrow \{-1, 1\}, \tag{41}$$

Given any natural number I, and real number $x \in [0, 1]$, we define the I_{th} Walsh Function as

$$W_I(x) = (-1)^{\sum_{k=0}^{\infty} x_k i_k}, \tag{42}$$

where i_j is the j_{th} bit in the binary representation of I, starting with i_0 as the least significant bit, and x_j is the j_{th} bit in the binary representation of x, starting with x_0 as the most significant fractional bit. Considering this definition we can therefore express the coefficient of the projector $|k\rangle\langle k|$ in the $\sigma_0^{i_0} ... \sigma_{n_Q-1}^{i_{n_Q-1}}$ element of the Cartan basis as

$$\frac{1}{N_x} W_I(x) \text{ where } I = \sum_{j=0}^{n_Q-1} i_j 2^j \text{ and } x = \sum_{j=0}^{n_Q-1} x_j 2^{-1-j}, \tag{43}$$

hence

$$|k\rangle\langle k| = \frac{1}{N_x} \sum_I W_I(x) \, \sigma_0^{i_0} ... \sigma_{n_Q-1}^{i_{n_Q-1}}. \tag{44}$$

E. Hamiltonian coefficients

In the previous section of the appendix we showed which are the coefficients of the Hamiltonian expressed in the Cartan basis, Eq. (19). Now we present how to chose the most significative of them. We discuss two cases: the Hermitan Hamiltonian $\hat{H}_{\mathrm{BSH}}$ and the embedded Hamiltonian $\tilde{H}$.

In the Hermitian case, every non-zero term has to include the interaction $\hat{\sigma}_0^z$ and the odd body interactions suppose in general the largest terms. For each non-zero term, Eq. (19) sums up to an analytical expression. We split the expressions into three categories: only first qubit interaction, interactions with an odd number of bodies, and interactions with an even number of bodies. Denoting by $0 = j_0 < j_1 < j_{2k} \leq n - 1$ the indices of the qubits on which the operators act, the reindexed coefficients h'_j of Eq. (19) are

$\underline{\hat{\sigma}_0^z\, \mathbb{I}_1 \dots\, \mathbb{I}_{n_Q-1}}$:

$$\frac{2^{n_Q}-1}{2^{n_Q+1}}\frac{2r-\sigma^2}{x_{\max}}\cot\left(\frac{\pi}{2^{n_Q}}\right). \tag{45}$$

$\underline{\hat{\sigma}_{j_0=0}^z\hat{\sigma}_{j_1}^z \dots\, \hat{\sigma}_{j_{2k}}^z}$:

$$(-1)^k\,\frac{2^{n_Q}-1}{2^{n_Q+1}}\frac{2r-\sigma^2}{x_{\max}}\cot\left(\frac{\pi}{2^{n_Q}}\right)\tan\left(\frac{\pi}{2^{j_1+1}}\right)\dots\,\tan\left(\frac{\pi}{2^{j_{2k}+1}}\right). \tag{46}$$

$\underline{\hat{\sigma}_{j_0=0}^z\hat{\sigma}_{j_1}^z \dots\, \hat{\sigma}_{j_{2k-1}}^z}$:

$$(-1)^k\,\frac{2^{n_Q}-1}{2^{n_Q+1}}\frac{2r-\sigma^2}{x_{\max}}\tan\left(\frac{\pi}{2^{j_1+1}}\right)\dots\,\tan\left(\frac{\pi}{2^{j_{2k-1}+1}}\right). \tag{47}$$

In the embedded case, the number of the interactions that play a relevant role, as seen in Fig 8, is minor, and every non-zero term has to discard the interaction $\hat{\sigma}_0^z$. Therefore we provide an approach for the largest terms: $\mathbb{I}_0 \dots\, \mathbb{I}_{n_Q-1}$ and $\mathbb{I}_0\hat{\sigma}_1^z\hat{\sigma}_2^z\mathbb{I}_3 \dots \mathbb{I}_{n_Q-1}$.

$\underline{\mathbb{I}_0 \dots\, \mathbb{I}_{n_Q-1}}$:

$$\frac{\pi}{2}-\frac{1}{2^{n_Q}}\sum_{k=0}^{2^{n_Q-1}}\left[\exp\left(-T\left(\frac{\sigma^2}{2}\frac{\sin^2(2\pi k/2^{n_Q})}{\delta_x^2}+r\right)\right)\right] \tag{48}$$

This is a good approach for $n_Q \geq 7$, and from $n_Q = 10$ due to the second term converges exponentially to 0 when $n_Q \to \infty$, its value can be taken as the constant $\frac{\pi}{2}$.

$\underline{\hat{\sigma}_1^z\hat{\sigma}_2^z\mathbb{I}_3 \dots \mathbb{I}_{n_Q-1}}$:

In this case, for $n_Q \geq 8$ the coefficient can be approached by

$$\frac{1}{2^{n_Q}}\left(2\arccos\left(\exp(-Tr)\right)-\pi\right)$$

$$+4\int_0^{\frac{1}{8}}\arccos\left(\exp\left(-T\left(\frac{\sigma^2}{2}\left(\frac{2^{n_Q}-1}{2x_{max}}\right)^2\sin(2\pi x)^2+r\right)\right)\right)dx$$

$$-4\int_{\frac{1}{8}}^{\frac{1}{4}}\arccos\left(\exp\left(-T\left(\frac{\sigma^2}{2}\left(\frac{2^{n_Q}-1}{2x_{max}}\right)^2\sin(2\pi x)^2+r\right)\right)\right)dx. \tag{49}$$

This term presents a decayment factor $\frac{1}{2^{n_Q}}$.

F. Index Degeneration

In this section we analyze the degeneration, $g_{I'}$ of the index $I' = \sum_{l=1}^{2k}(j_l-1)$ with $0 = j_0 < j_1 < j_{2k} \leq n_Q-1$, section V D. The problem is equivalent to solve the number of subsets of $X = \{0, \dots n_Q-2\}$ of an even number of elements for which the sum of the members is I'. As proposed in [52], the number of partitions of a positive integer I' into distinct parts, each $\leq n_Q-2$ is upper bounded by

$$g_{I'} < \left(\frac{2}{n_Q^2-3n_Q+4-4I'}+\frac{\pi}{2\sqrt{3I'}}\right)e^{(\pi/\sqrt{3}-e^{-\pi\frac{\left[\frac{n_Q-2}{2}\right]\sqrt{3}}{\pi\sqrt{3I'}}})\sqrt{I'}}$$

$$\leq \left(\frac{2}{n_Q^2-3n_Q+4}+\frac{\pi}{2\sqrt{3}}\right)e^{\pi/\sqrt{3}\sqrt{I'}} \tag{50}$$

for $I' \leq \frac{n_Q}{4}(n_Q-1)$. Considering that this degeneration distribution is symmetric respect to the middle, where it reaches the maximum value, we can conclude that

$$g_{I'} < 2\left(\frac{2}{n_Q^2-3n_Q+4}+\frac{\pi}{2\sqrt{3}}\right)e^{\pi/\sqrt{3}\sqrt{\frac{n_Q}{4}(n_Q-1)}} \tag{51}$$

where the factor 2 comes from the inclusion of the interactions with an even number of bodies. In order to simplify the notation, we define

$$C' = 2\left(\frac{2}{n_Q^2-3n_Q+4}+\frac{\pi}{2\sqrt{3}}\right)e^{\pi/\sqrt{3}\sqrt{\frac{n_Q}{4}(n_Q-1)}}C. \tag{52}$$

G. Truncation Error

In this section, we detail the calculations to obtain an upper for the truncation error. We consider the propagator corresponding to the excluded terms and compare it with the identity operator, thus

$$\left\|e^{iT\sum_{I'=M}^{\frac{n_Q}{2}(n_Q-1)-1}\sum_{J|I'(J)=I'}h'_J\hat{c}_J}-e^{i\theta}\mathbb{I}\right\|_\infty = \max_i|\lambda_i| \tag{53}$$

where λ_i is the ith eigenvalue of $e^{iT\sum_{I'=M}^{\frac{n_Q}{2}(n_Q-1)-1}\sum_{J|I'(J)=I'}h'_J\hat{c}_J}-e^{i\theta}\mathbb{I}$.

Now, we proceed to upper bound the eigenvalues $|\lambda_i| = |\beta_i - 1|\ \forall i$, where β_i is the ith eigenvalue of $e^{iT\sum_{I'=M}^{\frac{n_Q}{2}(n_Q-1)-1}\sum_{J|I'(J)=I'}h'_J\hat{c}_J}$. In the worst case escenario, the maximum rotation angle between two eigenstates β_i and β_j, is $2\sum_{I'=M}^{\frac{n_Q}{2}(n_Q-1)-1}\sum_{J|I'(J)=I'}|h'_J| \leq 2C\sum_{I'=M}^{\frac{n_Q}{2}(n_Q-1)-1}\frac{g_{I'}}{2^{I'}} < 2\frac{2C'}{2^M}$, with C' a new constant depending on n_Q and the financial parameters (see Appendix VII F). Taking M sufficiently large to guarantee that $C'e^{-\log(2)M} \leq \pi/4$, this angle difference is minor than π and evenly distributed around the real axis, hence the optimal gauge election is $\theta = 0$. Thus, we can conclude that $\max_i|\lambda_i| \leq |e^{iT\frac{2C'}{2^M}}-1| = \sqrt{2\left(1-\cos(2TC'e^{-\log(2)M})\right)}$, and therefore it is straighforward to obtain Eq. (25) .

Given the inequality for the truncation error, we now calculate an upper bound for the index M for a given $\epsilon \in [0,1]$ to satisfy such error.

$$\epsilon \leq \sqrt{2\left(1-\cos(2TC'e^{-\log(2)M})\right)}, \tag{54}$$

$$\cos\left(2TC'2^{-M}\right) \leq 1 - \frac{\epsilon^2}{2}, \tag{55}$$

due to $\arccos(x)$ it is a decreasing function in $[\frac{1}{2}, 1]$

$$\arccos\left(1 - \frac{\epsilon^2}{2}\right) \leq 2TC'2^{-M}, \tag{56}$$

and then

$$M \leq \log_2\left[\frac{1}{2TC'}\arccos\left(1 - \frac{\epsilon^2}{2}\right)\right]^{-1}$$

$$= \log_2(2TC') + \log_2(\arccos(1 - \epsilon^2/2)). \tag{57}$$

H. Comparison to classical methods for solving PDEs

As a part of our study, we have also analyzed the performance of our quantum algorithm compared to classical techniques usually employed to solve Black Scholes PDE. In this context, Crank-Nicolson arises as the standard finite difference method used for numerically solving the heat equation. In contrast to our algorithm, this method discretizes time, it is second-order method in time, what indeed supposes an extra limitation in the accuracy of the solution. Relative error of quantum algorithm and Crank-Nicolson solutions respect to analytical are shown in Fig. 11. As we can observe, there is an asymptotic constant behaviour in Crank-Nicolson associated with the limitation introduced by time discretization.

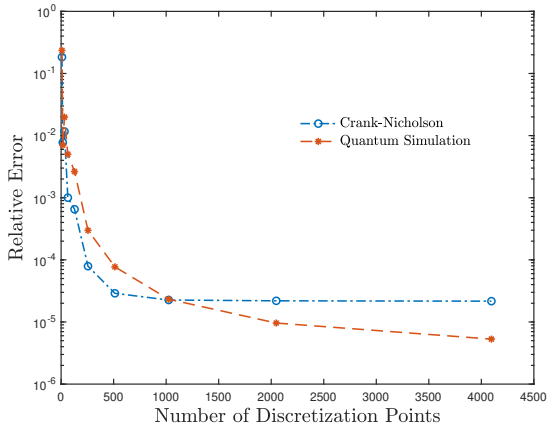

FIG. 11. Comparison of the accuracy reached for Crank-Nicolson scheme and the quantum algorithm. Crank-Nicolson shows better results when the number of discretization points is low, but time discretization effects limit this method when the grid has over 1000 points and we can appreciate how this technique gets stuck. In the opposite side, quantum algorithm improves its accuracy continuously as we enlarge the grid size.

I. Hamiltonian Implementation Circuit Details

In this section we show the quantum circuit implementing the Hamiltonian for the solution proposed in Fig. 5 with 8+2 qubits considering largest 14 Hermitian + 6 embedded interactions. We omit the already explained blocks of the circuit performing initialization, Quantum Fourier Transform and measurement.

In order to implement the non-Hermitian Hamiltonian dynamics we use an extra set of gates {Z,S,H}. First, in order to produce the embedding we need to use the $\hat{\sigma}^z$=Z=$\begin{pmatrix}1 & 0\\ 0 & -1\end{pmatrix}$ gate acting on q_E as we can see in Eq. (6). Then, we make use of the property Y=SHZHS†, where S=$\begin{pmatrix}1 & 0\\ 0 & i\end{pmatrix}$, H=$\frac{1}{\sqrt{2}}\begin{pmatrix}1 & 1\\ 1 & -1\end{pmatrix}$, $\hat{\sigma}^y$=Y=$\begin{pmatrix}0 & -i\\ i & 0\end{pmatrix}$, to transform $e^{i\beta\,(\hat{\sigma}^z_{i_1}\ldots.\,\hat{\sigma}^z_{i_k})\otimes\hat{\sigma}^y_E}$ into S†H$e^{i\beta\,(\hat{\sigma}^z_{i_1}\ldots.\,\hat{\sigma}^z_{i_k})\otimes\hat{\sigma}^z_E}$HS for every term in the exponential of the non-Hermitian Hamiltonian. Finally, for both Hamiltonians, we implement every exponential $e^{i\beta\,(\hat{\sigma}^z_{i_1}\ldots.\,\hat{\sigma}^z_{i_k})\otimes\hat{\sigma}^z_E}$ term as a β phase rotation whose sign depends on the parity of the state that is computed by using controlled NOT gates. There exists several alternatives to compute the parity of a state, in particular we chose to add an ancillary qubit q_G that tracks this property. This election leads to the cancelation of some controlled NOT gates if we chose a proper order for the terms to be implemented. Each one of the boxed labeled operators acting on ancillary qubit q_G, consist on a phase rotation toward z axis, the value of the angle rotation is given by the coefficient of the corresponding boxed vector. $C_{\hat{H}}$ denotes the Cartan vectors representation of the Hermitian Hamiltonian and $C_{\tilde{H}}$ the Cartan basis of the embedded decomposition.

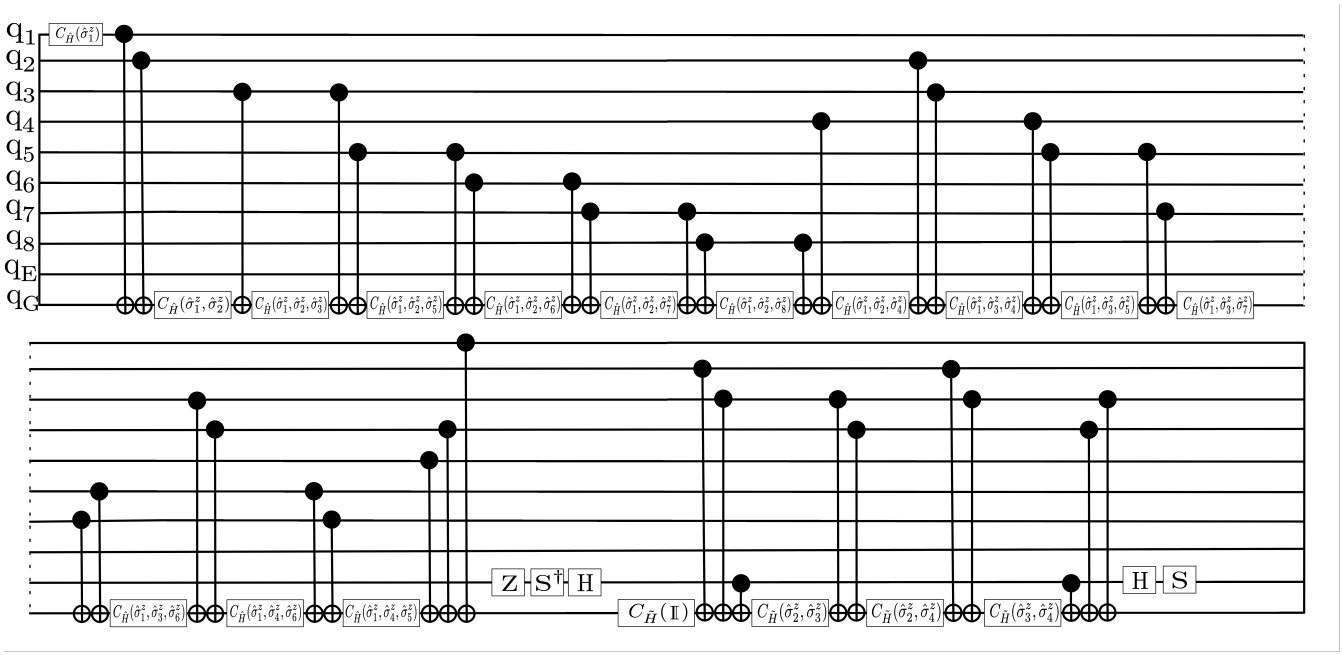

FIG. 12. Circuit gates implementation of Hermitian Hamiltonian and embedded dynamics proposed with 8 qubit and the 14+6 largest body interactions. Each one of the boxed labeled operators acting on ancillary qubit q_G, consist on a phase rotation toward z axis, the value of the angle rotation is given by the coefficient of the corresponding boxed vector. $C_{\hat{H}}$ denotes the Cartan vectors of the Hermitian Hamiltonian and $C_{\tilde{H}}$ the basis of the embedded decomposition.

[1] F. Black and M. Scholes, *The Pricing of Options and Corporate Liabilities*. The Journal of Political Economy **81**, 637 (1973).

[2] R.Valkov, *Fitted Finite Volume Method for a Generalized Black-Scholes Equation Transformed on Finite Interval*. ArXiv:1211.1903 (2012).

[3] J. A. Acebron, *A Monte Carlo method for computing the action of a matrix exponential on a vector*. ArXiv:1904.12759 (2019).

[4] W. C. Chen and W. H. Chung, *Option Pricing via Multi-path Autoregressive Monte Carlo Approach*. 61st Meeting of EURO Working Group for Commodities and Financial Modeling, 16-18 MAY 2018, Kaunas, Lithuania.

[5] G. Krzyżanowski, M. Magdziarz, and Ł. Płociniczak, *A weighted finite difference method for subdiffusive Black Scholes Model*. ArXiv:1907.00297 (2019).

[6] G. Krzyżanowski and M. Magdziarz, *A computational weighted finite difference method for American and barrier options in subdiffusive Black-Scholes model*. ArXiv:2003.05358 (2020).

[7] F. Arute, K. Arya, R. Babbush *et al*, *Quantum supremacy using a programmable superconducting processor*. Nature **574**, 505 (2019).

[8] D. J. Egger, C. Gambella, J. Marecek, S. McFaddin, M. Mevissen, R. Raymond, A. Simonetto, S. Woerner, and E. Yndurain, *Quantum computing for Finance: state of the art and future prospects*. IEEE Transactions on Quantum Engineering (2020).

[9] R. Orús, S. Mugel, and E. Lizaso, *Quantum computing for finance: Overview and prospects*. Reviews in Physics **4**, 100028 (2019).

[10] R. Orús, S. Mugel, and E. Lizaso, *Forecasting financial crashes with quantum computing*. Phys. Rev. A **99**, 060301(R) (2019).

[11] Y. Ding, J. Gonzalez-Conde, L. Lamata, J. D. Martín-Guerrero, E. Lizaso, S. Mugel, X. Chen, R. Orús, E. Solano, and M. Sanz, *Towards Prediction of Financial Crashes with a D-Wave Quantum Computer*. ArXiv:1904.05808 (2019).

[12] A. Martin, B. Candelas, A. Rodríguez-Rozas, J. D. Martín-Guerrero, X. Chen, L. Lamata, R. Orús, E. Solano, and M. Sanz, *Towards Pricing Financial Derivatives with an IBM Quantum Computer*. ArXiv:1904.05803 (2019).

[13] D. Venturelli and A. Kondratyev, *Reverse quantum annealing approach to portfolio optimization problems*. Quantum Mach. Intell. (2019)

[14] P. Rebentrost and S. Lloyd, *Quantum computational finance: quantum algorithm for portfolio optimization*. ArXiv:1811.03975 (2018).

[15] S. Mugel, C. Kuchkovsky, E. Sanchez, S. Fernandez-Lorenzo, J. Luis-Hita, E. Lizaso, and R. Orús, *Dynamic Portfolio Optimization with Real Datasets Using Quantum Processors and Quantum-Inspired Tensor Networks*. ArXiv:2007.00017 (2020).

[16] J. Cohen, A. Khan, and C. Alexander, *Portfolio Optimization of 40 Stocks Using the D-Wave Quantum Annealer*. ArXiv:2007.01430 (2020).

[17] J. Cohen, A. Khan, and C. Alexander, *Portfolio Optimization of 60 Stocks Using Classical and Quantum Algorithms*. ArXiv:2008.08669 (2020).

[18] B. Coyle, M. Henderson, J. C. J. Le, N. Kumar, M. Paini, and E. Kashefi, *Quantum versus Classical Generative Modelling in Finance*. ArXiv:2008.00691 (2020).

[19] H. Tang, A. Pal, L. F. Qiao, T. Y. Wang, J. Gao, and X. M. Jin, *Quantum Computation for Pricing the Collateral Debt Obligations*. ArXiv:2008.04110 (2020).

[20] L. Braine, D. J. Egger, J. Glick, and S. Woerner, *Quantum Algorithms for Mixed Binary Optimization applied to Transaction Settlement*. ArXiv:1910.05788 (2019).

[21] S. Woerner and D. J. Egger, *Quantum risk analysis*. Npj Quantum Inf **5**, 15 (2019).

[22] D. J. Egger, R. G.Gutiérrez, J. C. Mestre, S. Woerner, *Credit Risk Analysis using Quantum Computers*. ArXiv:1907.03044 (2019).

[23] P. Rebentrost, B. Gupt, and T. R. Bromley, *Quantum computational finance: Monte Carlo pricing of financial derivatives*. Phys. Rev. A **98**, 022321 (2018).

[24] N. Stamatopoulos, D. J. Egger, Y. Sun, C. Zoufal, R. Iten, N. Shen, and S. Woerner, *Option Pricing using Quantum Computers*. Quantum **4**, 291 (2020).

[25] D. Grinko, J. Gacon, C. Zoufal, and S. Woerner, *Iterative Quantum Amplitude Estimation*. ArXiv:1912.05559 (2019).

[26] S. Chakrabarti, R. Krishnakumar, G. Mazzola, N. Stamatopoulos, S. Woerner, and W. J. Zeng, *A Threshold for Quantum Advantage in Derivative Pricing*. ArXiv:2012.03819 (2020).

[27] S. Ramos-Calderer, A. Pérez-Salinas, D. García-Martín, C. Bravo-Prieto, J. Cortada, J. Planagumà, and J. I. Latorre, *Quantum unary approach to option pricing*. ArXiv:1912.01618 (2019).

[28] A. Montanaro and S. Pallister, *Quantum algorithms and the finite element method*. Phys. Rev. A **93**, 032324 (2016).

[29] A. M. Childs, J. Liu, and A. Ostrandertextit, *High-precision quantum algorithms for partial differential equations*. ArXiv:2002.07868 (2020).

[30] T. Xin, S. Wei, J. Cui, J. Xiao, I. Arrazola, L. Lamata, X. Kong, D. Lu, E. Solano, and G. Long, *Quantum algorithm for solving linear differential equations: Theory and experiment*. Phys. Rev. A **101** 032307 (2020).

[31] R. Di Candia, B. Mejia, H. Castillo, J. S. Pedernales, J. Casanova, and E. Solano, *Embedding Quantum Simulators for Quantum Computation of Entanglement*. Phys. Rev. Lett. **111**, 240502 (2013).

[32] D. W. Berry, G. Ahokas, R. Cleve, and B. C. Sanders, *Efficient quantum algorithms for simulating sparse Hamiltonians*. Comm. Math. Phys. **270**, 359 (2007).

[33] A. M. Childs, D. Maslov, Y. Nam, N. J. Ross, and Y. Su, *Toward the first quantum simulation with quantum speedup*. PNAS **115**, 9456 (2018).

[34] D. W. Berry, A. M. Childs, and R. Kothari, *Hamiltonian simulation with nearly optimal dependence on all parameters*. FOCS, pp. 792 (2015).

[35] P. C. S. Costa, S. Jordan, and A. Ostrander, *Quantum Algorithm for Simulating the Wave Equation*. Phys. Rev. A **99**, 012323 (2019).

[36] A. Suau, G. Staffelbach, and H. Calandra, *Practical Quantum Computing: solving the wave equation using a quantum approach*. ArXiv:2003.12458 (2020).

[37] L. Jin and Z. Song, *Physics counterpart of the PT non-Hermitian tight-binding chain*. Phys. Rev. A **81**, 032109 (2010).

[38] B. E. Baaquie, *Quantum Finance Hamiltonians and Path Integrals for Options* (Cambridge University Press, Cambridge, 2004).

[39] T. Constantinescu, *Schur Parameters, Dilation and Factorization Problems*. Vol **82**, (Birkhäuser Verlag, 1996),

[40] N. Klco and M. J. Savage, *Digitization of Scalar Fields for*

Quantum Computing. Phys. Rev. A **99**, 052335 (2019).

[41] M. Plesch and Č. Brukner, *Quantum state preparation with universal gate decompositions.* Phys. Rev. A **83**, 032302 (2011).

[42] A. Macridin, P. Spentzouris, J. Amundson, and R. Harnik, *Digital quantum computation of fermion-boson systems*. Phys. Rev. A **98**, 042312 (2018).

[43] M. Möttönen, J. J. Vartiainen, V. Bergholm, and M. M. Salomaa, *Transformation of quantum states using uniformly controlled rotations*. Quant. Inf. Comp. **5**, 467 (2005)

[44] V.V. Shende, S. S. Bullock, and I. L. Markov, *Synthesis of Quantum Logic Circuits*. IEEE Trans. on Computer-Aided Design, vol. **25**, (2006)

[45] N.J. Ward, I. Kassal, and A. Aspuru-Guzik, *Preparation of many-body states for quantum simulation*. J. Chem. **Phys**. 130, 194105 (2009)

[46] A. C. Vazquez and S.Woerner, *Efficient State Preparation for Quantum Amplitude Estimation*. ArXiv:2005.07711 (2020).

[47] M. Schuld and F. Petruccione, *Supervised Learning with Quantum Computers*. OCLC: 1076208411 (2019).

[48] L. Grover and T. Rudolph, *Creating superpositions that correspond to efficiently integrable probability distributions*. ArXiv: quant-ph/0208112 (2002).

[49] J. J. García-Ripoll, *Quantum-inspired algorithms for multivariate analysis: from interpolation to partial differential equation*. ArXiv:1909.06619 (2019)

[50] C. Zoufal, A. Lucchi, and S. Woerner, *Quantum generative adversarial networks for learning and loading random distributions*. Npj Quantum Information **5**, 1–9 (2019).

[51] M. A. Nielsen and I. L. Chuang, *Quantum Computation and Quantum Information* (Cambridge University Press, Cambridge, 2000).

[52] M. Bidar *Partition of an Integer into Distinct Bounded Parts,Identities and Bounds*. Integers, **12**, 445, (2012).